


Article

Structural Aspects and Intermolecular Energy for Some Short Testosterone Esters

Alexandru Turza ¹, Violeta Popescu ², Liviu Mare ² and Gheorghe Borodi ^{3,*} 

¹ Mass Spectrometry, Chromatography and Applied Physics Department, National Institute for R&D of Isotopic and Molecular Technologies, 67-103 Donat, 400293 Cluj-Napoca, Romania

² Physics & Chemistry Department, Technical University of Cluj-Napoca, 28 Memorandumului Str., 400114 Cluj-Napoca, Romania

³ Molecular and Biomolecular Physics Department, National Institute for R&D of Isotopic and Molecular Technologies, 67-103 Donat, 400293 Cluj-Napoca, Romania

* Correspondence: borodi@itim-cj.ro

Abstract: Testosterone (17 β -hydroxyandrost-4-en-3-one) is the primary naturally occurring anabolic-androgenic steroid. The crystal structures of three short esterified forms of testosterone, including propionate, phenylpropionate, and isocaproate ester, were determined via single-crystal X-ray diffraction. Furthermore, all the samples were investigated using powder X-ray diffraction, and their structural features were described and evaluated in terms of crystal energies and Hirshfeld surfaces. They were also compared with the base form of testosterone (without ester) and the acetate ester. Moreover, from a pharmaceutical perspective, their solubility was evaluated and correlated with the length of the ester.

Keywords: 17 β -hydroxyandrost-4-en-3-one; testosterone; ester; crystal structure; lattice energy; solubility



Citation: Turza, A.; Popescu, V.; Mare, L.; Borodi, G. Structural Aspects and Intermolecular Energy for Some Short Testosterone Esters. *Materials* **2022**, *15*, 7245. <https://doi.org/10.3390/ma15207245>

Academic Editors: Nikolaos Bouropoulos and Fabien Delpech

Received: 9 September 2022

Accepted: 13 October 2022

Published: 17 October 2022

Publisher's Note: MDPI stays neutral with regard to jurisdictional claims in published maps and institutional affiliations.



Copyright: © 2022 by the authors. Licensee MDPI, Basel, Switzerland. This article is an open access article distributed under the terms and conditions of the Creative Commons Attribution (CC BY) license (<https://creativecommons.org/licenses/by/4.0/>).

1. Introduction

Testosterone (17 β -hydroxyandrost-4-en-3-one) is a cholesterol derivative and a naturally occurring anabolic steroid. It can be viewed as a derivative of the androstane group and the primary male sex hormone. It plays a major role in the development of male reproductive tissues and the maintenance of secondary male characteristics [1]. Testosterone has been shown to impact overall health and well-being [2] and prevent osteoporosis [3]. By binding to the androgen receptor, it exerts anabolic and androgenic properties that are the specific common characteristic of all derivatives belonging to this class [4]. In a medical context, testosterone is used to relieve symptoms of low testosterone in men (male hypogonadism) and breast cancer in women, as well as for hormone therapy in transgender men [5]. Testosterone targets androgen receptors [6], and previous studies have shown that normal testosterone levels in older men have an overall positive impact on health, decreasing body and visceral fat, increasing lean body mass, and improving cholesterol panel and carbohydrate metabolism [7]. Since it is an anabolic-androgenic steroid, testosterone is often used by athletes to increase performance [8]. Furthermore, medically, it can be used to relieve or treat protein degradation in certain catabolic states [9].

It is known that the testosterone base (Figure 1) has a short half-life of roughly a few hours; thus, it is often subjected to esterification in order to increase the half-life by intramuscular injections and avoid daily administration [10]. The esterified forms of testosterone possess a half-life ranging from around less than 1 day for testosterone acetate, 1 day for propionate, 2.5 days for phenylpropionate, and up to 3.1 days for testosterone isocaproate [11]. In this regard, the length of the ester can be correlated with the length of the carbon chain; thus, the longer the ester, the longer the half-life.

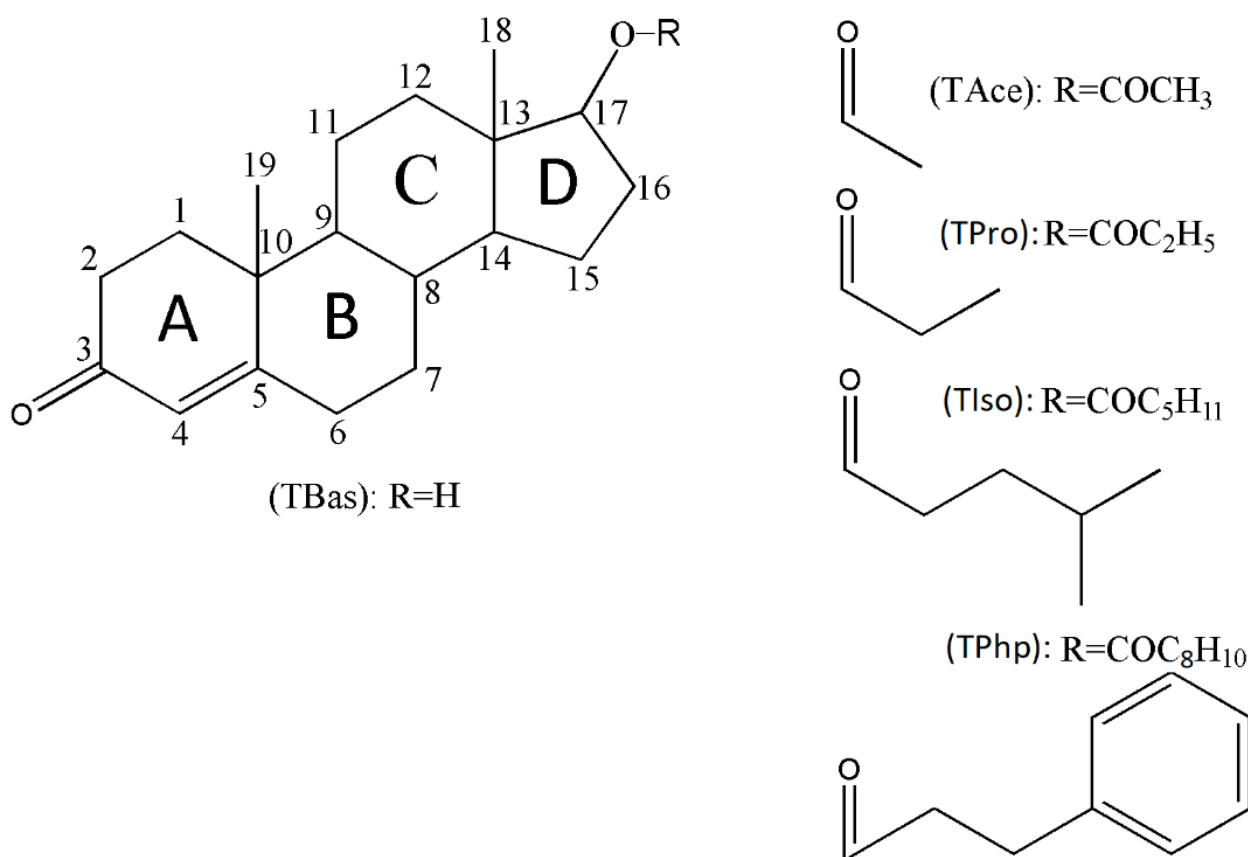


Figure 1. Chemical structures of 17 β -hydroxyandrost-4-en-3-one (testosterone) displaying the steroid backbone labelling system and other studied testosterone-based steroids.

The scheme of atoms and the labelling of steroid skeleton rings was made according to the established notations for the compounds belonging to this group [12] (Figure 1).

The current study aimed to investigate the characterisation of four testosterone pro-drugs as follows:

- (i) Testosterone acetate (Androst-4-en-17 β -ol-3-one 17 β -acetate; TAce);
- (ii) Testosterone propionate (Androst-4-en-17 β -ol-3-one 17 β -propionate; TPro);
- (iii) Testosterone isocaproate (Androst-4-en-17 β -ol-3-one 17 β -4-methylpentanoate; TIso);
- (iv) Testosterone phenylpropionate (Androst-4-en-17 β -ol-3-one 17 β -phenylpropionate; TPhp).

For the last three, the crystal structures were determined and reported.

The literature reports the crystal structure of a form of testosterone propionate that has a slightly different unit cell and does not have the positions of the hydrogen atoms reported [13], and another paper presents only the approximate parameters of the unit cell [14]. Other testosterone-based crystal structures that have been reported are testosterone buclate [15], testosterone acetate [16], and testosterone base (the basic form without ester attached) [17]. This manuscript is aimed to investigate the structural features of these testosterone esters.

A complete structural characterisation was carried out by means of X-ray single-crystal diffraction (for TPro, TPhp, TIso), X-ray powder diffraction, and the conformational analysis of steroid rings, and a quantitative measure of intermolecular interactions was accomplished by computation of lattice energies using the Coulomb–London–Pauli model corroborated with Hirshfeld surface analysis. Furthermore, computational methods were also applied to the testosterone base in order to be compared with the four esters.

As many pharmaceutical compounds, including various esterified forms of steroids, are labelled as poorly water-soluble but lipophilic agents, they might be dissolved in

lipid-based preparations [18]. Based on this, the solubility in solutions of various organic oils was measured. The formulations of various drugs are currently available on the market, and all use oils as vehicles for certain compounds, including deoxycorticosterone, progesterone/oestradiol esters, testosterone esters with their analogues/derivatives, and vitamins such as K and E as well [19,20].

2. Materials and Methods

2.1. Materials and Crystallisation Experiments

Crystalline, white powders of esters for scientific research purposes, were received from Wuhan Shu Mai Technology Co., Wuhan, China and solvents from Merck, Taufkirchen, Germany.

All the investigated steroids were obtained at room temperature as white crystalline powders, which possess the possibility to be subjected to various recrystallisation methods. Suitable single crystals for X-ray data collection were successfully obtained in alcohols: methanol (TPro), ethanol (Tiso), and isopropyl alcohol (TPhp).

Oils meeting the requirements of United States Pharmacopeia were received from Sigma-Aldrich (Taufkirchen, Germany), Tex Lab supply (USA), and Med Lab supply (USA).

2.2. X-ray Powder Diffraction (XRPD)

The samples were scanned on a Bruker D8 Advance diffractometer (Karlsruhe, Germany) having the X-ray tube set at 40 kV and 40 mA. The diffractometer is equipped with a germanium (1 1 1) monochromator used to obtain only the desired CuK α 1 radiation and an LYNXEYE position-sensitive detector. X-ray diffraction patterns were recorded in the 3–40° (2 θ) range using the DIFFRAC plus XRD Commander program, employing a scanning speed of 0.02°/s.

2.3. Single-Crystal X-ray Diffraction and Structural Refinement

The experimental single-crystal X-ray diffraction intensities were collected using a SuperNova diffractometer (Rigaku, Tokyo, Japan) equipped with dual microsources (Mo and Cu) and the X-ray tube operating at 50 kV and 0.8 mA. Data collection and reduction, Lorentz, polarisation, and absorption effect corrections were all performed with CrysAlis PRO software (Yarnton, Oxfordshire, UK) [21]. A multi-scan method using spherical harmonics in the SCALE3 abspack algorithm was applied for the empirical absorption correction. The crystal structures were solved as follows: Tiso and TPhp were solved with SHELXT [22] program using intrinsic phasing, and TPro was solved with direct methods by SHELXS [23]. Steroid structures were further refined via least squares minimisation with SHELXL [24] refinement package, and all programs were incorporated into Olex2 software (Durham, UK) [25].

Hydrogen atoms were geometrically located, treated, and refined as riding atoms, with the isotropic displacement parameter $U_{iso}(H) = 1.2 U_{eq}(C)$ for ternary CH groups (C–H = 0.93 Å), secondary CH₂ groups (C–H = 0.97 Å), and 1.5 $U_{eq}(C)$ considered for all methyl CH₃ groups (C–H = 0.96 Å).

2.4. Crystal Lattice Energy Computation and Hirshfeld and Fingerprint Plot Analyses

Based on the positions of atoms in the unit cell (determined by single-crystal X-ray diffraction technique), the classical atom–atom potential was calculated using the Coulomb–London–Pauli (CLP) model (Milan, Italy) [26]. The method evaluates crystal energies that can be divided into three distinct attraction terms, namely Coulombic, polarisation, and dispersion energies, and a fourth term that represents the repulsive component.

Energy computation via the Coulomb–London–Pauli (CLP) approach involves pairs of individual atoms (i, j) that belong to different molecules and is the sum of four interaction terms according to Relation (1):

$$E_{ij} = 1/(4\pi\epsilon_0)(q_i q_j) R_{ij}^{-1} - F_P P_{ij} R_{ij}^{-4} - F_D D_{ij} R_{ij}^{-6} + F_R T_{ij} R_{ij}^{-12} \quad (1)$$

$$q_i = F_Q q_i^0 \quad (2)$$

The Coulombic energy is the first term, polarisation energy is the second term, the dispersion term is the third one, and the last term is repulsion.

The F_Q , F_P , F_D , and F_R coefficients involved in Relations (1) and (2) are empirically disposable scaling parameters and the P_{ij} , D_{ij} , and T_{ij} coefficients depend on the local vicinity of the atom in the molecule.

The Coulombic component is treated according to Coulomb's law, the polarisation term is estimated in the approximation of the linear dipole, the dispersion energy is approximated as the inverse of the distance at the sixth power, and the repulsive term is due to the modulation of the overlapping wave function.

Molecular 3D Hirshfeld surfaces and their related 2D fingerprint plots were generated by CrystalExplorer software (Perth, Australia) [27] based on the d_{norm} function, which can be expressed in Relation (3).

$$d_{norm} = \frac{d_i - r_i^{vdW}}{r_i^{vdW}} + \frac{d_e - r_e^{vdW}}{r_e^{vdW}} \quad (3)$$

where d_e is the distance from the surface to the nearest external nucleus, while d_i represents the distance from the surface to the nearest nucleus inside the surface. The fingerprint plots are a 2D diagram, where d_i and d_e are represented in order to identify the nature and types of different intermolecular contacts [28].

2.5. Solubility Check

The solubility for the four esters (mg/mL) was measured in solutions of various organic oils: medium-chain triglyceride (MCT), grape seed oil (GSO), castor oil, cottonseed oil, apricot oil, and sesame oil.

Each solution was composed of a mixture of benzyl benzoate, benzyl alcohol, and oil having a volumetric ratio of 78% oil, 20% benzyl benzoate, and 2% benzyl alcohol. In various pharmaceutical preparations of lipophilic compounds, including various steroids, benzyl benzoate is used as a solubiliser (co-solvent), benzyl alcohol acts as a solvent and at the same time prevents microbial growth and increases the lipid solubility of various esterified compounds, while the oils are used as carriers.

The solubility evaluation was performed in multiple steps at room temperature (25 °C) by successively adding small amounts of raw materials (2–5 mg each step), and the solution was stirred for up to several hours until dissolved. When it was found that excess raw material remained (in suspension), small amounts of solution (mixture of benzyl benzoate, benzyl alcohol, and oil) were added until the resulting solution became perfectly transparent and clear. In order to obtain good accuracy, three such procedures were carried out, and their average was used.

3. Results and Discussion

3.1. Crystal Structures and Supramolecular Descriptions

The good agreement generated between the experimental powder X-ray diffraction patterns and the simulated patterns based on the positions of the atoms in the unit cell shows a good structural homogeneity and that the studied single crystals are representative of the entire bulk of samples (see Figure S1, Supplementary Materials).

The details with regard to single-crystal data and refinement for the studied esters are given in Table 1.

Table 1. Crystal structures and refinement data of investigated esters.

Identification Code	TPro (Testosterone Propionate)	TIso (Testosterone Isocaproate)	TPhp (Testosterone Phenylpropionate)
Empirical formula	C ₂₂ H ₃₂ O ₃	C ₂₅ H ₃₈ O ₃	C ₂₈ H ₃₆ O ₃
Formula weight	344.47	386.57	420.57
Temperature/K	293(2)	293(2)	293(2)
Crystal system	orthorhombic	monoclinic	monoclinic
Space group	P2 ₁ 2 ₁ 2 ₁	P2 ₁	P2 ₁
a/Å	7.57470(16)	7.2877(3)	13.4097(7)
b/Å	12.6768(2)	12.3741(5)	5.9105(3)
c/Å	20.4038(4)	13.1272(6)	15.4054(8)
α/°	90	90	90
β/°	90	103.305(4)	95.073(5)
γ/°	90	90	90
Volume/Å ³	1959.23(6)	1152.02(9)	1216.22(11)
Z	4	2	2
ρ _{calc} /cm ³	1.168	1.106	1.148
μ/mm ^{−1}	0.594	0.552	0.568
F(000)	752.0	418.0	456.0
Crystal size/mm	0.09 × 0.08 × 0.07	0.1 × 0.03 × 0.01	0.09 × 0.09 × 0.01
Radiation	CuKα (λ = 1.54184)	CuKα (λ = 1.54184)	CuKα (λ = 1.54184)
2θ range/°	8.212 to 141.254	9.952 to 141.104	5.76 to 141.522
Index ranges	−8 ≤ h ≤ 9, −15 ≤ k ≤ 15, −24 ≤ l ≤ 24	−8 ≤ h ≤ 8, −15 ≤ k ≤ 15, −15 ≤ l ≤ 16	−16 ≤ h ≤ 16, −7 ≤ k ≤ 7, −18 ≤ l ≤ 18
Reflections collected	28,102	15,810	14,176
Independent reflections	3723 [R _{int} = 0.0243, R _{sigma} = 0.0119]	4322 [R _{int} = 0.0246, R _{sigma} = 0.0185]	4529 [R _{int} = 0.0796, R _{sigma} = 0.0508]
Data/restraints/ parameters	3723/0/229	4322/1/257	4529/1/282
Goodness-of-fit on F ²	1.044	1.076	1.078
Final R indexes [I ≥ 2σ (I)]	R ₁ = 0.0421, wR ₂ = 0.1187	R ₁ = 0.0621, wR ₂ = 0.1739	R ₁ = 0.0762, wR ₂ = 0.1784
Final R indexes [all data]	R ₁ = 0.0440, wR ₂ = 0.1217	R ₁ = 0.0740, wR ₂ = 0.1900	R ₁ = 0.1102, wR ₂ = 0.1959
Largest diff. peak/hole/e Å ^{−3}	0.17/−0.17	0.33/−0.21	0.25/−0.21
Flack parameter	0.04(6)	0.06(8)	−0.4(3)

The aim was to determine the absolute configurations for each of the testosterone esters investigated. The values of Flack parameters of 0.04(6) for TPro and 0.06(8) for TIso confirm the correctness of the absolute configurations; on the other hand, for TPhp, the negative value of the Flack parameter shows that this parameter has no meaning.

3.1.1. TAc (Testosterone Acetate)

The acetate ester is the shortest esterified steroid ester available and is also the shortest testosterone ester available. The CSD database contains one entry reporting only the cell parameters for this particular testosterone ester [16] and one entry reporting the unit cell parameters and atomic coordinates [14].

The acetate ester was found to crystallise in the noncentrosymmetric orthorhombic P2₁2₁2₁ space group with one molecule in the asymmetric unit (Figure S2a, Supplementary Materials) and four in the unit cell. The carbonyl O1 oxygen of the ketone group is involved in C-H...O bifurcated hydrogen bonds and contributes to crystal stability. One is made with a neighbouring five-membered ring (C15-H15A...O3) and one towards the CH₃ of

terminal methyl in the acetate group (Figure S2b, Supplementary Materials). Hydrogen bonding distances are presented in Table S1 (Supplementary Materials).

3.1.2. TPro (Testosterone Propionate)

Compared with testosterone acetate, the propionate ester is characterised by an ester chain with an extra carbon atom. The crystal structure of propionate ester was previously reported [13] but has slightly smaller unit cell parameters and lacks hydrogen atoms. Similar to TAc, it crystallises in the orthorhombic $P2_12_12_1$ space group, with one molecule in the asymmetric unit (Figure 2a), the unit cell hosting four such molecules. Considering the H atoms located in idealised positions via X-ray crystallography, apparently, it seems that only the C6-H6B \cdots O1 interaction between the O1 ketone group and the neighbouring D ring in the structure has a separating distance shorter than the sum of van der Waals radii and plays a role in stability. In reality, having the H atoms normalised (the C-H distance is 1.089 Å), the ketone O1 oxygen is involved in bifurcated C-H \cdots O interactions, with the second being C16-H16A \cdots O1 with $d(\text{H}\cdots\text{O}) = 2.6185$ Å. This distance is close to the sum of the van der Waals radii with 1.20 Å for hydrogen and 1.52 Å for oxygen [29]. An overall packing perspective is shown in Figure 2b.

3.1.3. TIso (Testosterone Isocaproate)

The asymmetric unit (Figure 3a) consists of only one steroid molecule and was found to crystallise in the noncentrosymmetric $P2_1$ monoclinic space group. Ketone O1 participates in the formation of supramolecular self-assemblies, being involved in the trifurcated C-H \cdots O hydrogen bonding. One interaction is formed between a neighbouring six-membered B ring (C6-H6B \cdots O1), one binds the O1 carbonyl oxygen with a five-membered ring (C16-H16B \cdots O1), while the last bridges the methyl CH₃ group (C19-H19A \cdots O1); all these interactions are detailed in Table S1 (Supplementary Materials). An overall packing diagram shows the self-arrangements of steroid molecules in layers (Figure 3b).

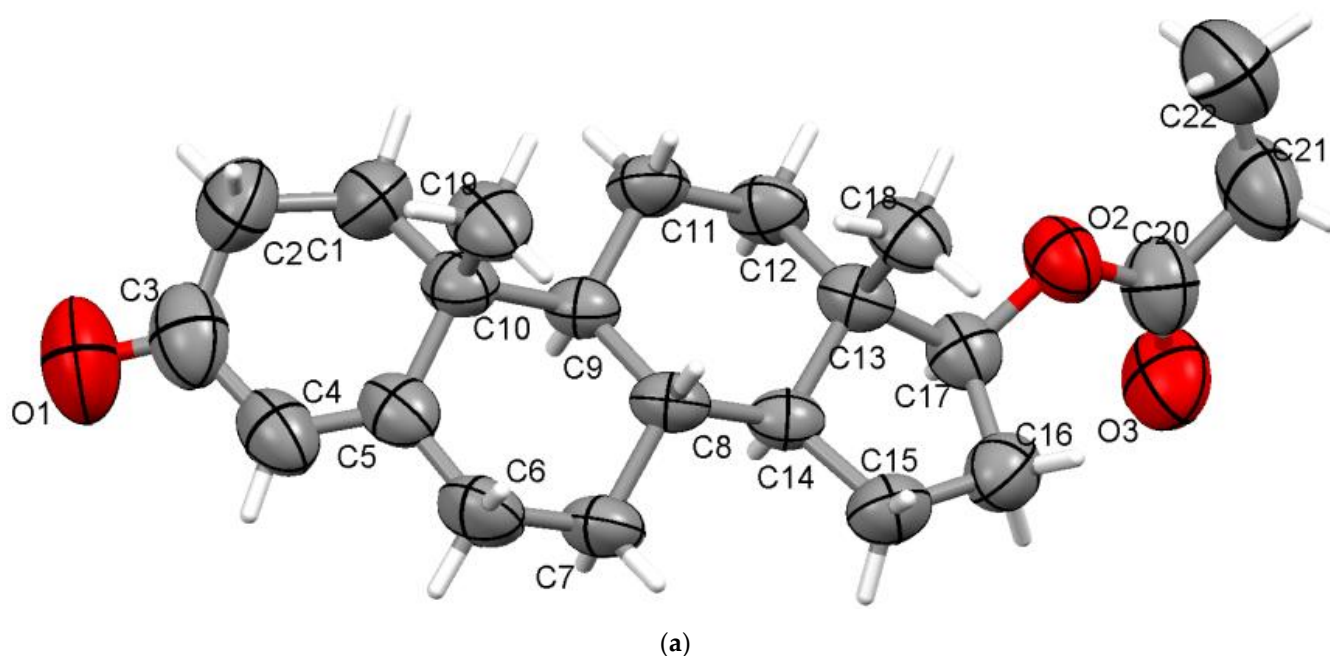


Figure 2. Cont.

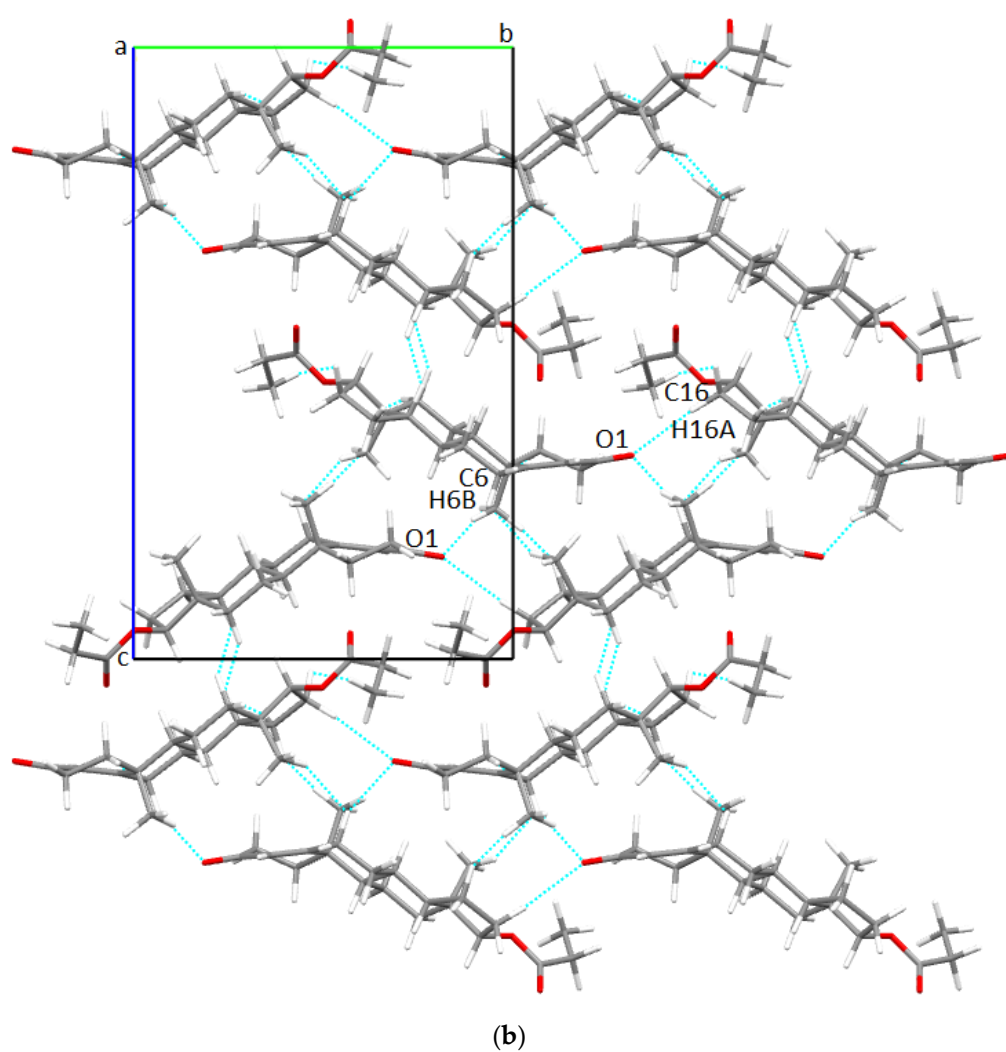


Figure 2. Asymmetric unit of TPro presenting nonhydrogen atoms at 50% probability level (a) and overall packing diagram along a-axis (b).

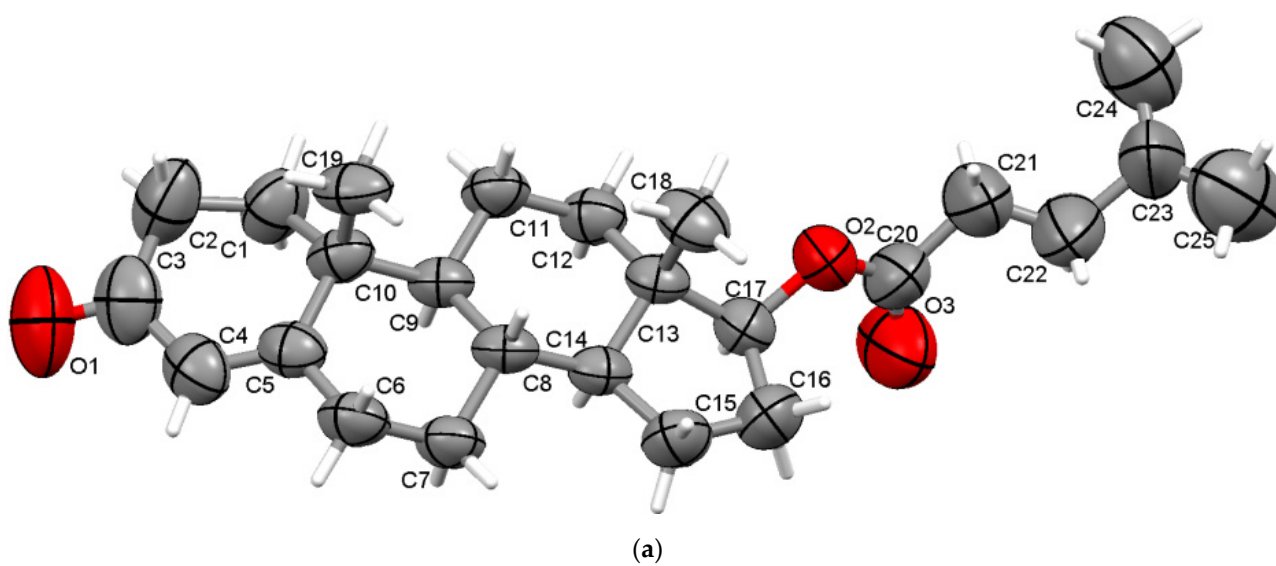


Figure 3. Cont.

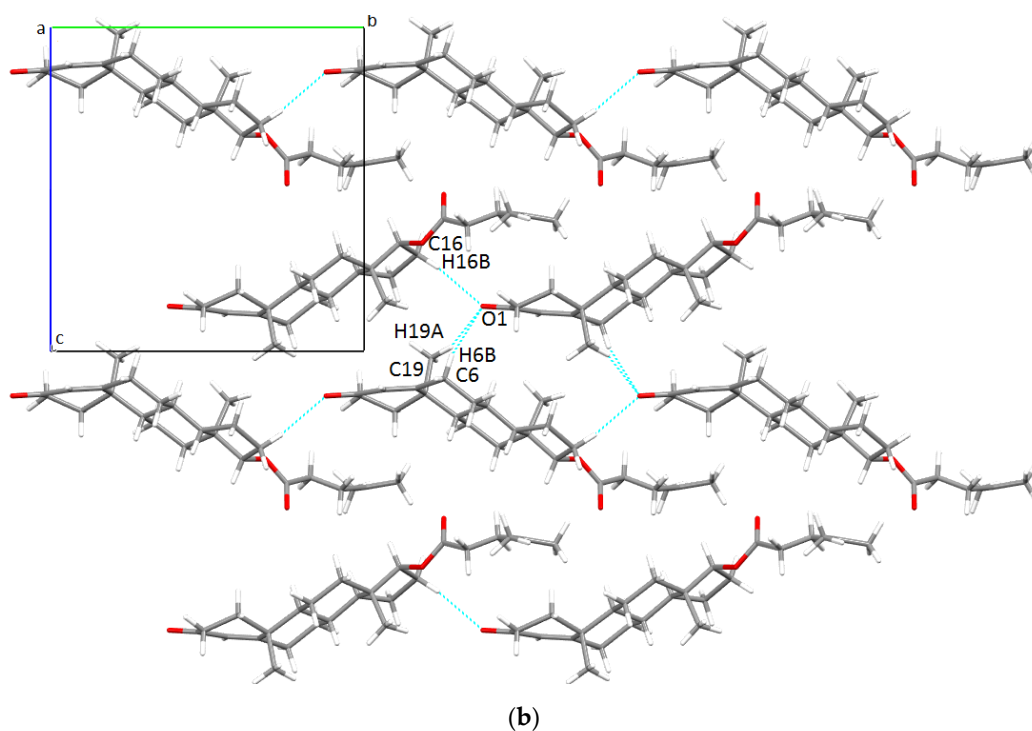


Figure 3. Asymmetric unit of Tlso presenting nonhydrogen atoms at 50% probability level (a) and overall packing diagram along a-axis (b).

3.1.4. TPhp (Testosterone Phenylpropionate)

It was found that the steroid crystallises in the monoclinic $P2_1$ space group with one molecule in the asymmetric unit (Figure 4a) and two in the unit cell. Similar to testosterone propionate, considering the H positions determined via X-ray diffraction, it seems only one C-H...O interaction exists in the crystal lattice (C24-H24...O1 between the terminal phenyl ring and the ketone O1 oxygen, Table S1) that is shorter than the sum of van der Waals radii. After the normalisation of the C-H distances, there is C2-H2A...O3 interaction between ring A and carbonyl O3 oxygen, which has $d(\text{H}\cdots\text{O}) = 2.714 \text{ \AA}$, situated just at the limit distance of 2.72 \AA [29]. The overall packing perspective of testosterone phenylpropionate is presented along the ob-axis (Figure 4b).

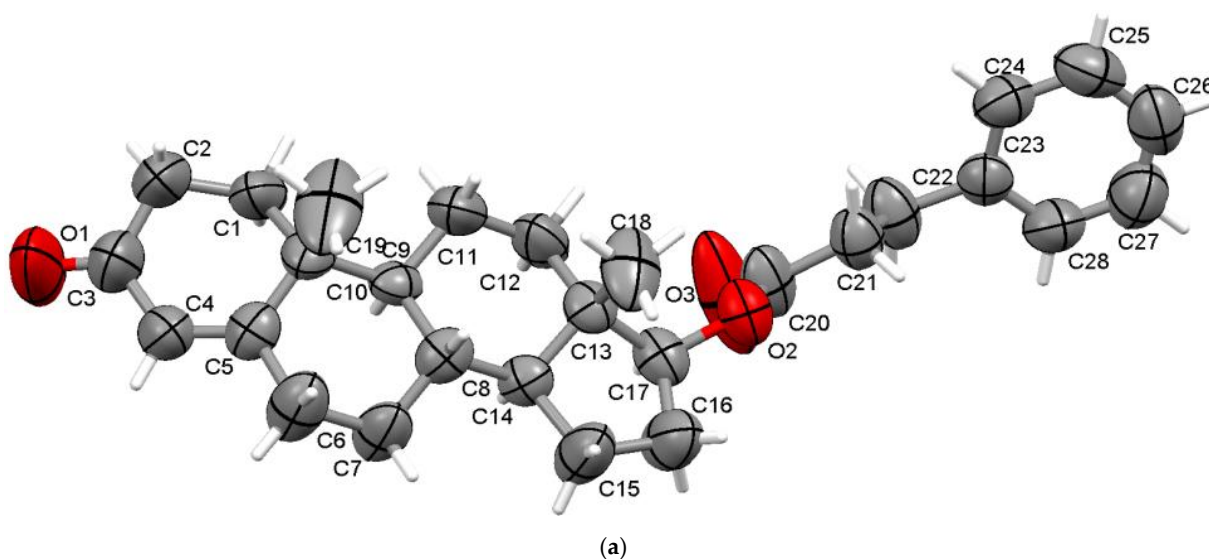


Figure 4. Cont.

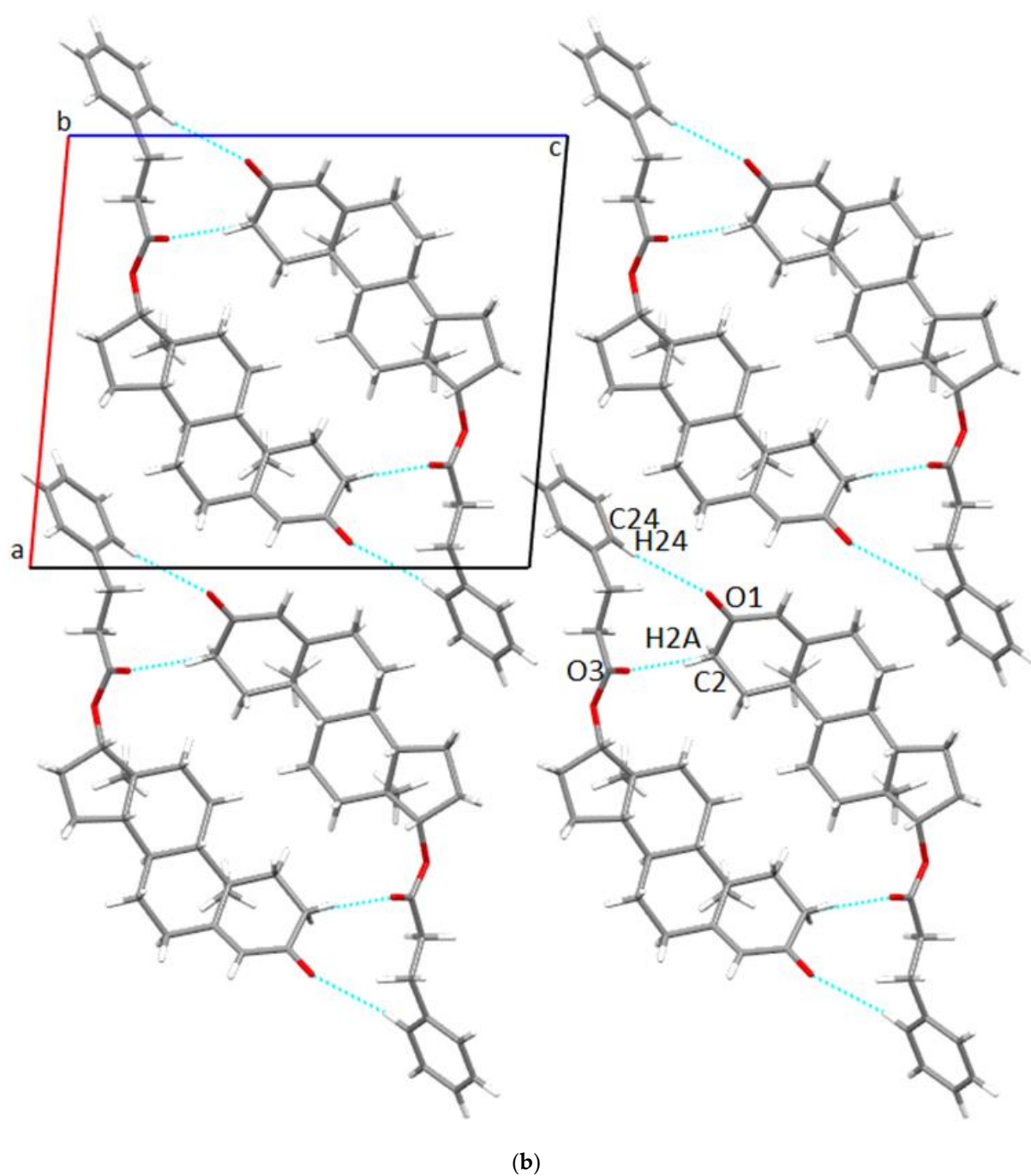


Figure 4. Asymmetric unit of TPhp presenting nonhydrogen atoms at 50% probability level (a) and overall packing diagram along b-axis (b).

From the analysis of the crystal structures, the following conclusions can be summarised:

- (i) Asymmetric units are characterised by a single molecule for each ester;
- (ii) The formations of supramolecular 3D assemblies are to some extent driven by the C-H...O interactions, although the dispersion energy has the greatest weight, as will be shown in the crystal energies analysis section; donor–acceptor separation distances show similar values to those of other crystals driven by C-H...O interactions and belong to the steroid family [30–34];
- (iii) The six-membered A rings are found in the intermediate sofa-half-chair geometry, and the B and C rings show chair conformations, while the five-membered D rings adopt

intermediate envelope-half-chair geometry. Similar geometries of skeleton rings have been reported in the crystal structure of its C-17 methylated form [35].

In Figure 5, the overlap of the molecular structures is exemplified. For example, (TPro, TPhp), which differ only by the extra phenyl ring of TPhp, show a totally different orientation of the tails, as in the case of the (TAce, TIso) pair as well. It can be seen that the part of the molecules representing testosterone, the base of the ester structures, overlaps very well in all pairs. Instead, there are differences in the orientation of carbon tails. Thus, for the pair (TPro, TPhp), the C17-O2-C20-O3 torsion angle is 2.89° for TPro and -3.78° for TPhp. The angle between the planes defined by the O3-C20-O2 atoms for the pair (TPro, TPhp) is 64.93° . For the pair (TAce, TIso), the C17-O2-C20-O3 torsion angle is 3.73° for TAce and 4.93° for TIso, and the angle between the planes defined by the O3-C20-O2 atoms for the two structures is 75.03° .

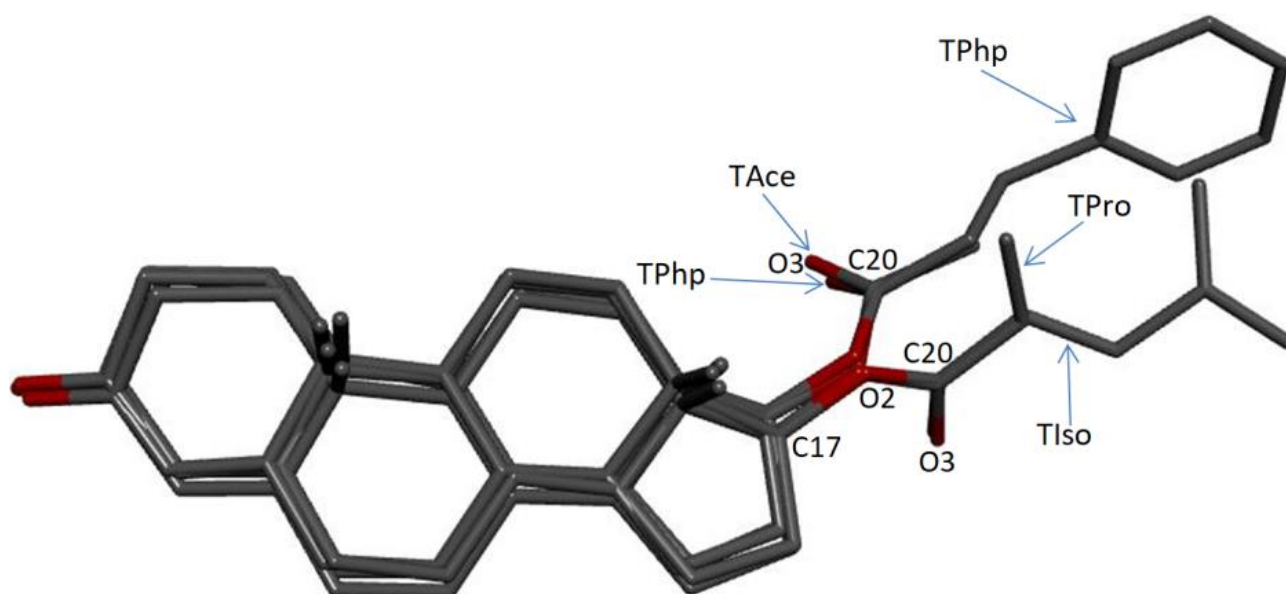


Figure 5. Molecular overlaps of the investigated esters.

The overlap of (TAce, TPhp) and (TPro, TIso) pairs show a better match; thus, the angle between the O3-C20-O2 planes is 25.35° for (TAce, TPhp) and 11.22° for (TPro, TIso).

3.2. Crystal Energy Analysis

The total crystal lattice energies, as well as the nature and magnitudes of the individual four energy components, were computed using the atom–atom Coulomb–London–Pauli model, and the results are shown in Table 2. Moreover, the energies of the four testosterone esters were compared with those of the testosterone base [17] deposited in CSD (denoted Tbas), which is not esterified.

All four steroid structures are characterised by large values of dispersion energies, and this component is dominant. As a general trend, the dispersion energies were found to be more significant, as the ester chain is longer; thus, TAce, which is the shorter ester, has a value of -126.1 kJ/mol, whereas TPhp, which represents the longest ester, is -149.0 kJ/mol.

Due to the fact that the structures lack strong hydrogen bonds, the Coulombic energy contributes the least in the crystal packings, with similar values through all the crystals, which are in the range of -15.5 kJ/mol for TAce and -21.3 kJ/mol for TIso. Carbonyl...hydrogen interactions were found in the Coulombic term and for the derivatives under study, the Coulombic energy has a weight between 9.7% (for TAce) and 12.6% (for TIso).

Table 2. Crystal energies of base form and its four esters.

Structure	Molar Mass g/mol	E_{coul} (kJ/mol)	E_{pol} (kJ/mol)	E_{disp} (kJ/mol)	E_{rep} (kJ/mol)	E_{latt} (kJ/mol)
TBas	288.43	−33.3	−47.5	−130.9	60.9	−150.8
TAce	330.46	−15.5	−55.0	−126.1	37.1	−159.5
TPro	344.49	−18.3	−55.5	−126.4	33.9	−166.3
TIso	386.57	−21.3	−57.7	−141.9	52.7	−168.2
TPhp	420.59	−19.3	−52.3	−149.0	36.1	−184.5

E_{coul} : the Coulombic term; E_{pol} : the polarisation term; E_{disp} : the dispersion term; E_{rep} : the repulsive term; E_{latt} : total crystal lattice energy.

By contrast, the Coulombic component (−33.3 kJ/mol) in the testosterone base (without ester), which presents strong classical O-H●●●O hydrogen bonds, contributes more to the lattice energy.

Polarisation and repulsive components do not display a particular trend, but on the other hand, the total lattice energy becomes lower as the steroid molecular mass increases. The shortest ester (TAce) has a total lattice energy of −159.5 kJ/mol and TPhp, which is the longest ester, has an energy of −184.5 kJ/mol and the most bound structure of all five steroids.

Similar crystal lattice behaviour in the sense that the dispersion term dominates the crystals, and the total energy becomes greater with the increase in ester length has been previously reported in other anabolic–androgenic agents from the steroid group [36–39].

3.3. Hirshfeld and Fingerprint Plot Analysis

The molecular 3D Hirshfeld surfaces of the studied esters (Figure S3b, Supplementary Materials) were generated based on d_{norm} and were compared with those of the base form (TBas) (Figure S3a, Supplementary Materials). As the asymmetric unit of TBas is characterised by two individual molecules, they were analysed separately.

The surfaces are interactively illustrated with arrows for the intermolecular C-H●●●O and O-H●●●O contacts with distances shorter than the sum of the van der Waals radii, which are listed in Table S1 (Supplementary Materials).

The surfaces can be understood by colour code; specifically, the red areas illustrate the intermolecular contacts with distances smaller than the sum of the van der Waals radii, the white indicates separation distances approximately equal to vdW radii, and the blue areas show the contacts with longer distances.

For each crystal, a 2D fingerprint plot (Figure 6) is generated, which is a transposition of the 3D Hirshfeld surface. The fingerprint plot of the base form (TBas) shows two fingerprint diagrams.

The analyses of 3D Hirshfeld surfaces, their related 2D fingerprint plots shapes, and (d_e and d_i) distances summarise the following structural features:

- Fingerprint plots of esterified forms (Figure 6b) (TAce, TPro, TPhp, and TIso) show symmetry in the spikes, which is a particular feature for the crystals with one molecule in asymmetric units, while the plots of TBas (Figure 6a) are asymmetric due to the different molecular environment in the crystal;
- The diagrams of TAce, TPro, and TIso illustrate protruding H●●●O/O●●●H spikes, denoting the presence of C-H●●●O hydrogen bonds, while for TPhp, the lack of H●●●O/O●●●H spikes shows that the separation distances of the C-H●●●O interactions fall in a range closer to the sum of vdW radii;
- The fingerprint plots of TBas show more protruding H●●●O/O●●●H spikes compared with its esterified forms and suggest that strong O-H●●●O interactions play more important roles in packing; this feature is seen in the evaluation of crystal energies where the Coulombic energy becomes more significant in TBas due to the presence of strong O-H●●●O contacts;

- (iv) The quantitative breakdown of fingerprint diagrams (Table 3) in all five crystals reveals a high percentage of $H\cdots H$ contacts, medium contribution by $O\cdots H/H\cdots O$ intercontacts and considerably smaller for $C\cdots H/H\cdots C$, respectively;
- (v) The large percentages in $H\cdots H$ contacts for all five structures (fingerprint plots breakdown in Table 3) corroborated with the crystal energies (Table 2) are suggesting that dispersion effects play the major role.

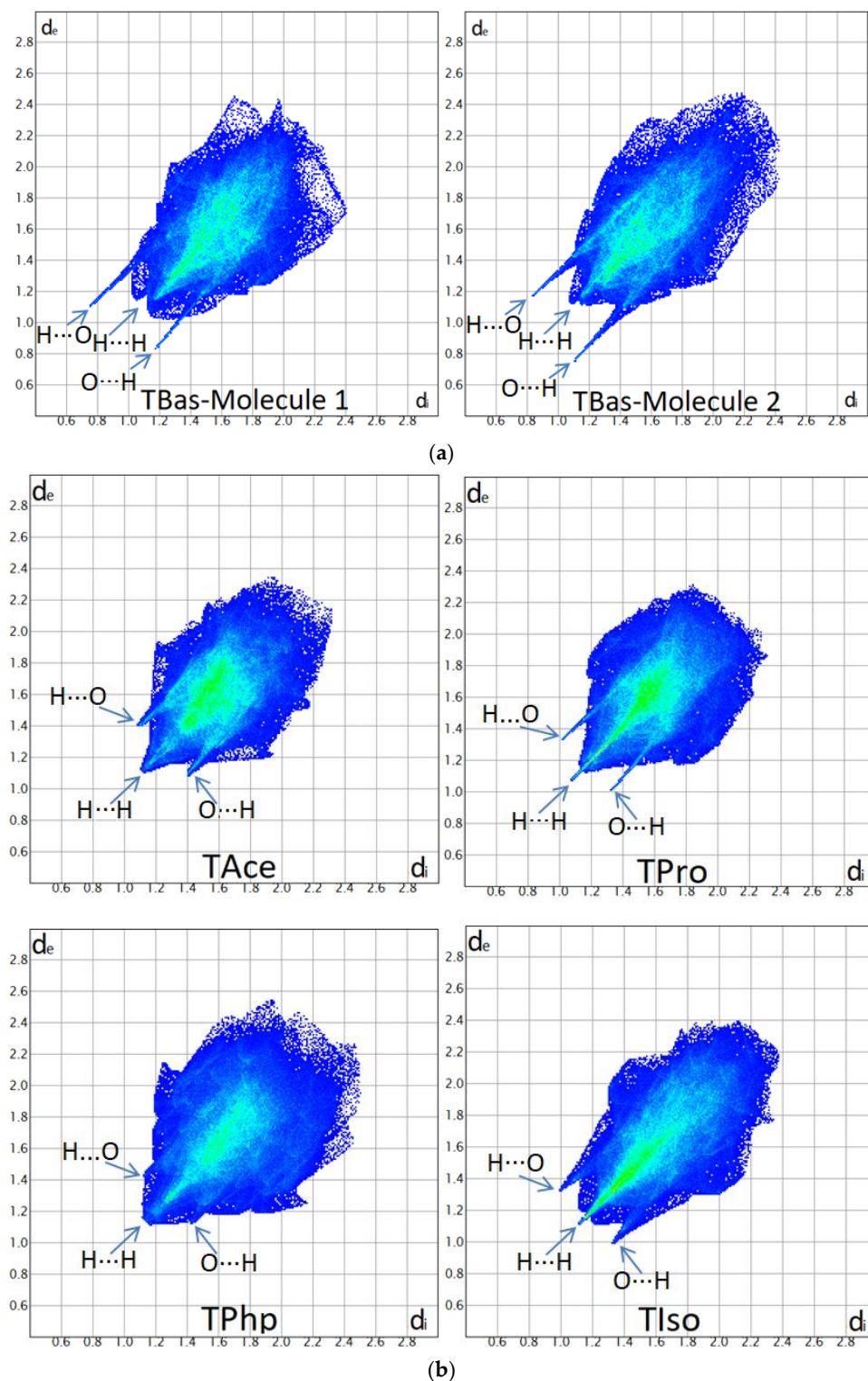


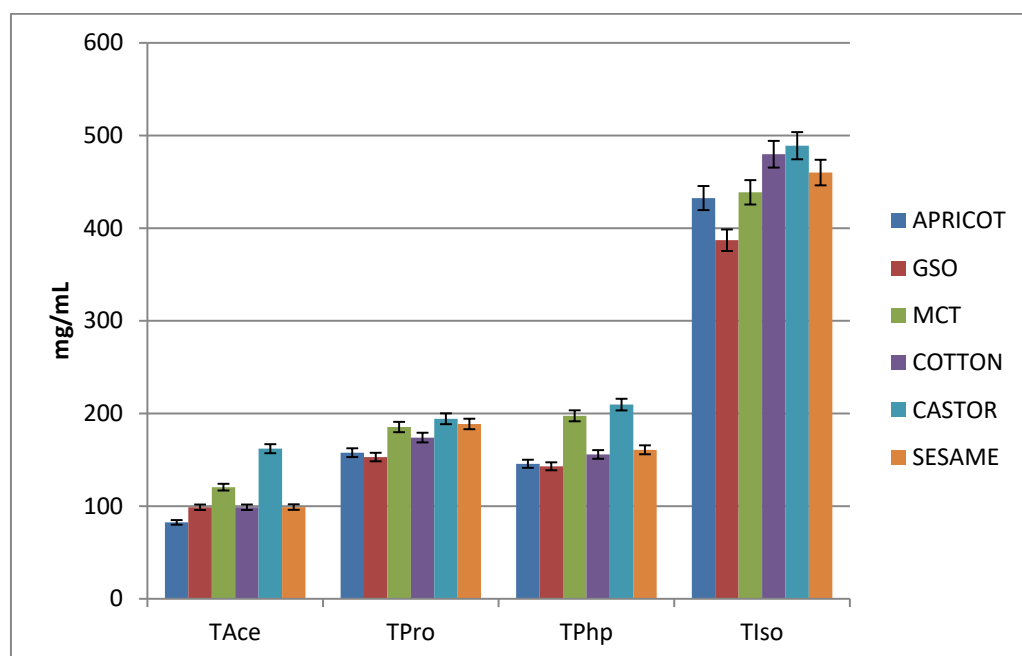
Figure 6. Fingerprint plots displaying close contacts in studied crystals: TBas (a) and studied esters (b).

Table 3. Contributions to the Hirshfeld surfaces for various intercontacts.

Structure	H...H	O...H/H...O	C...H/H...C	C...O/O...C	O...O	C...C
TBas Mol A	78.8%	17.2%	4.0%	-	-	-
TBas Mol B	76.4%	19.7%	3.9%	-	-	-
TAce	75.4%	20.2%	2.8%	1.2%	-	0.4%
TPro	76.5%	19.4%	4.0%	-	0.1%	-
TIso	80.4%	16.3%	3.3%	-	-	-
TPhp	72.7%	15.2%	12.1%	-	-	-

3.4. Solubility Check

The values obtained by solubility evaluation are summarised in Table S2 (Supplementary Materials) and are graphically represented in Figure 7.

**Figure 7.** Graphical representations of ester solubility.

Depending on the length of the ester, it is observed that the shortest ester (the acetate) has the lowest solubility, while the longest ester (isocaproate) has a roughly four-fold greater solubility. Propionate and phenylpropionate esters have similar and slightly higher values than acetate. Although phenylpropionate has six more carbon atoms than propionate, the solubilities are similar, so it can be noted that what matters in increasing solubility is the length of the chain (the phenyl ring does not lead to an increase in solubility).

It is worth mentioning that solubility correlates with the half-life of the prodrug, so acetate, which has the shortest half-life, has the lowest solubility, and isocaproate, which has the longest half-life, has the highest solubility.

Out of the six mixtures analysed, it is observed that castor oil can support the highest solubility without crashing (crystallisation of compound) and to a lesser extent MCT (for TAce, TPro, and TPhp), at the same time behaving as solvents as well. This is interesting because MCT is characterised by the lowest value of the viscosity coefficient, while castor oil is the most viscous.

The literature reports the solubility of hydroxyprogesterone caproate polymorphs in castor oil at a temperature of 20 °C, which are 278 mg/mL and 301 mg/mL [40]. Another

method used for the development of the preparations of drugs with poor water solubility (including various esterified forms of steroids) is by oil-in-water (*o/w*) microemulsions. For example, a previous study shows that a microemulsion based on soybean oil and dimethoxytetraethylene glycol supports concentrations of 3.42 mg/mL (for testosterone propionate), 31.5 mg/mL (for testosterone enanthate), and 2.16 mg/mL (for medroxyprogesterone acetate) in soybean oil. In dimethoxytetraethylene glycol, higher concentrations of 12 mg/mL (for testosterone propionate) 91.2 mg/mL (for testosterone enanthate) and 1.32 mg/mL (for medroxyprogesterone acetate) were obtained [41].

4. Conclusions

The crystal structures of three testosterone-based esters (propionate, phenylpropionate, and isocaproate) were determined; they belong to the noncentrosymmetric monoclinic $P2_1$ and orthorhombic $P2_12_12_1$ space groups.

These three esters were further analysed and compared with the acetate ester and with the nonesterified base form. Backbone steroid rings possess similar geometry in all compounds, the A steroid rings adopt intermediate sofa-half-chair conformations, and the B and C rings have chair conformations, while ring D depicts an intermediate envelope-half-chair conformation. By overlapping the esters, a very good match of the steroid skeleton rings (the base of the ester structures) emerges, and the major structural differences are manifested in the orientation of the tails.

Computational methods showed that in all crystal structures, the supramolecular arrangements and crystal stability are characterised and assured by dominant dispersion effects, and the total lattice energies are greater in absolute terms, as the ester chain is longer, while C-H...O hydrogen bonds in all esters play a less important role.

The solubility of the four derivatives was tested to evaluate the changes based on the added ester functionalities, and it was found that the shortest ester (acetate) has the lowest solubility, while the longest ester (isocaproate) is roughly four times greater; meanwhile, propionate and phenylpropionate are between the two and show similar values.

Supplementary Materials: The following supporting information can be downloaded at: <https://www.mdpi.com/article/10.3390/ma15207245/s1>, Figure S1: Experimental and simulated XRPD patterns comparison: TAc (a), TPro (b), TIso (c), TPhp (d); Figure S2: Asymmetric unit of TAc presenting non-hydrogen atoms at 50% probability level (a) Overall packing diagram along a-axis (b); Figure S3: Views of the Hirshfeld surfaces mapped with d_{norm} illustrating the intermolecular contacts referred in Table S1: TBas (a) and studied esters (b); Table S1: Hydrogen bond geometry for analyzed crystals (\AA , $^\circ$); Table S2: Solubility of analyzed testosterone esters in various oil solutions. CIF files of studied esters have been deposited with the Cambridge Crystallographic Data Centre with the deposition numbers as follows: 2192706 (TPro); 2192707 (TIso); 2192708 (TPhp). Copies of them can be obtained free of charge on written application to CCDC, 12 Union Road, Cambridge CB2 1EZ, UK (fax: +44-12-2333-6033); on request via e-mail to deposit@ccdc.cam.ac.uk or by access to <http://www.ccdc.cam.ac.uk> (accessed on 9 September 2022).

Author Contributions: Conceptualisation, A.T. and G.B.; methodology, G.B.; software, A.T.; validation, G.B., L.M. and V.P.; formal analysis, L.M.; investigation, A.T., G.B., L.M. and V.P.; resources, A.T. and G.B.; data curation, G.B.; writing—original draft preparation, A.T., V.P. and L.M.; writing—review and editing, A.T.; visualisation, G.B.; supervision, V.P.; project administration, V.P.; funding acquisition, A.T. and G.B. All authors have read and agreed to the published version of the manuscript.

Funding: This research was funded by the Romanian Ministry of Research and Innovation, grant number 19 35 02 02.

Institutional Review Board Statement: Not applicable.

Informed Consent Statement: Not applicable.

Data Availability Statement: Data is contained within the article or supplementary material.

Conflicts of Interest: The authors declare no conflict of interest.

References

1. Mooradian, A.D.; Morley, J.E.; Korenman, S.G. Biological actions of androgens. *Endocr. Rev.* **1987**, *8*, 1–28. [\[CrossRef\]](#) [\[PubMed\]](#)
2. Bassil, N.; Alkaade, S.; Morley, J.E. The benefits and risks of testosterone replacement therapy: A review. *Ther. Clin. Risk Manag.* **2009**, *5*, 427–448. [\[CrossRef\]](#) [\[PubMed\]](#)
3. Tuck, S.P.; Francis, R.M. Testosterone, bone and osteoporosis. *Front. Horm. Res.* **2009**, *37*, 123–132. [\[CrossRef\]](#) [\[PubMed\]](#)
4. Luetjens, C.M.; Weinbauer, G.F. *Chapter 2: Testosterone: Biosynthesis, Transport, Metabolism and (Non-Genomic) Actions*, 4th ed.; Cambridge University Press: Cambridge, UK, 2012; pp. 15–32.
5. Pappas, I.I.; Craig, W.Y.; Spratt, L.V.; Spratt, D.I. Efficacy of Sex Steroid Therapy Without Progestin or GnRH Agonist for Gonadal Suppression in Adult Transgender Patients. *J. Clin. Endocrinol. Metab.* **2021**, *106*, E1290–E1300. [\[CrossRef\]](#)
6. Quigley, C.A.; Bellis, A.D.; Marschke, K.B.; Awady, M.K.; Wilson, E.M.; French, F.S. Androgen receptor defects: Historical, clinical, and molecular perspectives. *Endocr. Rev.* **1995**, *16*, 271–321. [\[CrossRef\]](#)
7. Stanworth, R.D.; Jones, T.H. Testosterone for the aging male; current evidence and recommended practice. *Clin. Interv. Aging.* **2008**, *3*, 25–44. [\[CrossRef\]](#)
8. Institute of Medicine (US). Committee on Assessing the Need for Clinical Trials of Testosterone Replacement Therapy. In *Testosterone and Aging: Clinical Research Directions*; National Academies Press: Washington, DC, USA, 2004.
9. Braunstein, G.D. The influence of anabolic steroids on muscular strength. *Princ. Med. Biol.* **1997**, *8*, 465–474. [\[CrossRef\]](#)
10. Vermeulen, A. Longacting steroid preparations. *Acta Clin. Belg.* **1975**, *30*, 48–55. [\[CrossRef\]](#)
11. Forsdahl, G.; Erced, D.; Geisendorfer, T.; Turkalj, M.; Plavec, D.; Thevis, M.; Tretzele, L.; Gmeiner, G. Detection of testosterone esters in blood. *Drug Test. Anal.* **2015**, *7*, 983–989. [\[CrossRef\]](#)
12. Elks, J.; Ganellin, C.R. *The Dictionary of Drugs: Chemical Data: Chemical Data, Structures and Bibliographies*, 1st ed.; Springer: Easton, PA, USA, 1990; p. 652.
13. Reisch, J.; Eki-Gucer, N.; Takacs, M.; Henkel, G. Photochemische Studien, 54. Photodimerisierung von Testosteronpropionat in kristallinem Zustand und Kristallstruktur von Testosteronpropionat. *Liebigs Ann. Der Chem.* **1989**, *1989*, 595–597. [\[CrossRef\]](#)
14. Griffiths, P.J.F.; James, K.C.; Rees, M. Crystallographic data for some testosterone esters. *Acta Cryst.* **1965**, *19*, 149. [\[CrossRef\]](#)
15. Alcock, N.W.; Sanders, K.J.; Rodger, A. Potential injectable contraceptive steroids: Testosterone buciclate. *Acta Cryst.* **2004**, *E60*, 348–349. [\[CrossRef\]](#)
16. Böcskei, Z.; Gérczei, T.; Bodor, A.; Schwartz, R.; Náray-Szabó, G. Three Testosterone Derivatives. *Acta Cryst.* **1996**, *C52*, 2899–2903. [\[CrossRef\]](#)
17. Roberts, P.J.; Pettersen, R.C.; Sheldrick, G.M.; Isaacs, N.W.; Kennard, O. Crystal and molecular structure of 17 β -hydroxyandrost-4-en-3-one (testosterone). *J. Chem. Soc. Perkin Trans.* **1973**, *2*, 1978–1984. [\[CrossRef\]](#)
18. Land, L.M.; Li, P.; Baummer, P.M. The Influence of Water Content of Triglyceride Oils on the Solubility. *Pharm. Res.* **2005**, *5*, 784–788. [\[CrossRef\]](#)
19. Remington. *The Science and Practice of Pharmacy*, 23rd ed.; Adejare, A., Ed.; Elsevier: Philadelphia, PA, USA, 2020.
20. Rowe, R.C.; Sheskey, P.J.; Quinn, M.E. (Eds.) *Handbook of Pharmaceutical Excipients*, 5th ed.; Pharmaceutical Press: London, UK; American Pharmacists Association: Washington, DC, USA, 2006.
21. CrysAlis PRO. Agilent Technologies UK Ltd., Oxford Diffraction; Agilent Technologies UK Ltd.: Yarnton, Oxfordshire, UK, 2015.
22. Sheldrick, G.M. SHELXT—Integrated space-group and crystal-structure determination. *Acta Cryst.* **2015**, *A71*, 3–8. [\[CrossRef\]](#)
23. Sheldrick, G.M. A short history of SHELX. *Acta Cryst.* **2008**, *A64*, 112–122. [\[CrossRef\]](#)
24. Sheldrick, G.M. Crystal structure refinement with SHELXL. *Acta Cryst.* **2015**, *C71*, 3–8. [\[CrossRef\]](#)
25. Dolomanov, O.V.; Bourhis, L.J.; Gildea, R.J.; Howard, J.A.K.; Puschmann, H. OLEX2: A complete structure solution, refinement and analysis program. *J. Appl. Cryst.* **2009**, *42*, 339–341. [\[CrossRef\]](#)
26. Gavezzotti, A. Efficient computer modeling of organic materials. The atom–atom, Coulomb–London–Pauli (AA-CLP) model for intermolecular electrostatic-polarization, dispersion and repulsion energies. *New J. Chem.* **2011**, *35*, 1360–1368. [\[CrossRef\]](#)
27. Turner, M.J.; McKinnon, J.J.; Wolff, S.K.; Grimwood, D.J.; Spackman, P.R.; Jayatilaka, D.; Spackman, M.A. *CrystalExplorer17*; University of Western Australia: The Nedlands, Australia, 2017.
28. Spackman, M.A.; McKinnon, J.J. Fingerprinting intermolecular interactions in molecular crystals. *CrystEngComm* **2002**, *4*, 378–392. [\[CrossRef\]](#)
29. Alvarez, S. A cartography of the van der Waals territories. *Dalton Trans.* **2013**, *42*, 8617–8636. [\[CrossRef\]](#) [\[PubMed\]](#)
30. Ohrt, J.; Haner, B.A.; Norton, D.A. Crystal data (II) for some androstanes. *Acta Cryst.* **1965**, *19*, 479. [\[CrossRef\]](#)
31. Turza, A.; Borodi, G.; Pop, M.M.; Ulici, A. Polymorphism and β -cyclodextrin complexation of methylrostanolone. *J. Mol. Struct.* **2022**, *1250*, 131852. [\[CrossRef\]](#)
32. Turza, A.; Ulici, A.; Pop, M.M.; Borodi, G. Solid forms and β -cyclodextrin complexation of turinabol. *Acta Cryst.* **2022**, *C78*, 305–313. [\[CrossRef\]](#)
33. Rajnikant, V.; Dinesh, D.; Aziz, N.; Gupta, B.D. Analysis of C–H \cdots O Intermolecular Interactions in 4-Androstene-3,17-dione. *J. Chem. Crystallogr.* **2009**, *39*, 24–27. [\[CrossRef\]](#)
34. Rajnikant, V.; Gupta, V.K.; Khan, E.H.; Shafi, S.; Hashmi, S.; Shafiullah, B. Varghese, Dinesh, Crystal structure of cholest-4-ene-3,6-dione: A steroid. *Crystallogr. Rep.* **2001**, *46*, 963–966. [\[CrossRef\]](#)
35. Gaedeck, Z. Structure of 17- α -methyl-testosterone semihydrate $C_{20}H_{30}O_2 \cdot \frac{1}{2} H_2O$. *J. Crystallogr. Spectrosc. Res.* **1989**, *19*, 577–587. [\[CrossRef\]](#)

-
36. Turza, A.; Miclaus, M.O.; Pop, A.; Borodi, G. Crystal and molecular structures of boldenone and four boldenone steroid esters. *Z. Kristallogr. Cryst. Mater.* **2019**, *234*, 671–683. [[CrossRef](#)]
 37. Borodi, G.; Turza, A.; Camarasan, P.A.; Ulici, A. Structural studies of Trenbolone, Trenbolone Acetate, Hexahydrobenzylcarbonate and Enanthate esters. *J. Mol. Struct.* **2020**, *1212*, 128127. [[CrossRef](#)]
 38. Borodi, G.; Turza, A.; Bende, A. Exploring the Polymorphism of Drostanolone Propionate. *Molecules* **2020**, *25*, 1436. [[CrossRef](#)] [[PubMed](#)]
 39. Turza, A.; Borodi, G.; Pop, A.; David, M. Structural studies of some androstane based prodrugs. *J. Mol. Struct.* **2022**, *1248*, 131440. [[CrossRef](#)]
 40. Caplette, J.; Frigo, T.; Jozwiakowski, M.; Shea, H.; Mirmehrabi, M.; Müller, P. Characterization of new crystalline forms of hydroxyprogesterone caproate. *Int. J. Pharm.* **2017**, *527*, 42–51. [[CrossRef](#)] [[PubMed](#)]
 41. Molcomson, C.; Lawrence, M.J. A comparison of incorporation of model steroids into non-ionic micellar and microemulsion systems. *J. Pharm. Pharmacol.* **1993**, *45*, 141–143. [[CrossRef](#)]